Technology in Cancer Research & Treatment
Volume 21: 1–11

DOI: 10.1177/15330338221078464
journals.sagepub.com/home/tct
SAGE

Performance Evaluation of Deformable Image Registration Algorithms Using Computed Tomography of Multiple Lung Metastases

Min Cheol Han, PhD[1], Jihun Kim, PhD[1], Chae-Seon Hong, PhD[1], Kyung Hwan Chang, PhD[2], Su Chul Han, PhD[1], Kwangwoo Park, PhD[1], Dong Wook Kim, PhD[1], Hojin Kim, PhD[1], Jee Suk Chang, MD[1], Jina Kim, MD[1], Sunsuk Kye, BS[3], Ryeong Hwang Park, MS[3], Yoonsun Chung, PhD[4], and Jin Sung Kim, PhD[1]

Abstract

Purpose: Various deformable image registration (DIR) methods have been used to evaluate organ deformations in 4-dimensional computed tomography (4D CT) images scanned during the respiratory motions of a patient. This study assesses the performance of 10 DIR algorithms using 4D CT images of 5 patients with fiducial markers (FMs) implanted during the postoperative radiosurgery of multiple lung metastases. **Methods:** To evaluate DIR algorithms, 4D CT images of 5 patients were used, and ground-truths of FMs and tumors were generated by physicians based on their medical expertise. The positions of FMs and tumors in each 4D CT phase image were determined using 10 DIR algorithms, and the deformed results were compared with ground-truth data. **Results:** The target registration errors (TREs) between the FM positions estimated by optical flow algorithms and the ground-truth ranged from 1.82 ± 1.05 to 1.98 ± 1.17 mm, which is within the uncertainty of the ground-truth position. Two algorithm groups, namely, optical flow and demons, were used to estimate tumor positions with TREs ranging from 1.29 ± 1.21 to 1.78 ± 1.75 mm. With respect to the deformed position for tumors, for the 2 DIR algorithm groups, the maximum differences of the deformed positions for gross tumor volume tracking were approximately 4.55 to 7.55 times higher than the mean differences. Errors caused by the aforementioned difference in the Hounsfield unit values were also observed. **Conclusions:** We quantitatively evaluated 10 DIR algorithms using 4D CT images of 5 patients and compared the results with ground-truth data. The optical flow algorithms showed reasonable FM-tracking results in patient 4D CT images. The iterative optical flow method delivered the best performance in this study. With respect to the tumor volume, the optical flow and demons algorithms delivered the best performance.

Keywords

deformable image registration, lung deformation, tumor tracking, fiducial marker tracking, multiple lung metastases

Abbreviations

IMRT, intensity-modulated radiation therapy; 4D CT, 4-dimensional computed tomography; FM, fiducial marker; DIR, deformable image registration; C-PAP, continuous positive airway pressure; GTV, gross tumor volume; HU, Hounsfield unit; DIRART, deformable image registration and adaptive radiotherapy; DVF, deformation vector field; TRE, target registration error

Received: October 19, 2021; Revised: November 29, 2021; Accepted: January 19, 2022.

[1] Yonsei University College of Medicine, Seoul, Republic of Korea
[2] Douzone, Seoul, Republic of Korea
[3] Yonsei Cancer Center, Seoul, Republic of Korea
[4] Hanyang University, Seoul, Republic of Korea

Corresponding Author:
Chae-Seon Hong, PhD and Jin Sung Kim, PhD, Yonsei University College of Medicine, 50-1 Yonsei-ro, Seodaemoon-gu, Seoul, South Korea.
Email: cs.hong@yuhs.ac; jinsung@yuhs.ac

Introduction

Intensity-modulated radiation therapy (IMRT) has become the standard technique in radiation therapy as an accurate and reliable dose delivery method for treating tumors, while sparing normal tissues from being affected by radiation.[1–4] While implementing IMRT, it is desirable to define the tumor volume as small as possible, but tumor movements due to respiratory motions disturb the clear delineation of the tumor volume.[5,6]

In this case, 4-dimensional computed tomography (4D CT) images are an effective option to provide information on the trajectories of tumors during respiratory motion,[7] and the real-time tumor tracking method based on a 4D CT-based plan is one of the most effective ways to deliver a high dose to a focal area while accounting for the respiratory motion.[8] Tumor tracking techniques mostly require the implant of fiducial markers (FMs) around the tumor as surrogates for the tumor position. However, in patients with small lung cancers (eg, oligometastases[9]), the implant of FMs before radiation treatment is clinically unacceptable due to the risk of pneumothorax up to 50%.[10]

Pop et al[11] suggested a new method, that is, peri-operative fiducial implant, for postoperative CyberKnife® (CyberKnife SRS, Accuray, Inc.) radiosurgery for the tumor-tracking treatment of lung tumor patients. For potential risks and local recurrences, they implanted preventive FMs near tumors during surgery, and the FMs were utilized for complementary radiation treatments. However, these methods can increase tumor

Table 1. Summary of Patient Characteristics.

	FMs			GTVs		
No.	Left	Right	Total	Left	Right	Total
Patient #1	3	3	6	5	5	10
Patient #2	3	2	5	0	2	2
Patient #3	2	3	5	0	1	1
Patient #4	2	2	4	2	1	3
Patient #5	3	3	6	1	4	5
Total	13	13	26	8	13	21

Abbreviations: FM, fiducial markers; GTV, gross tumor volume.

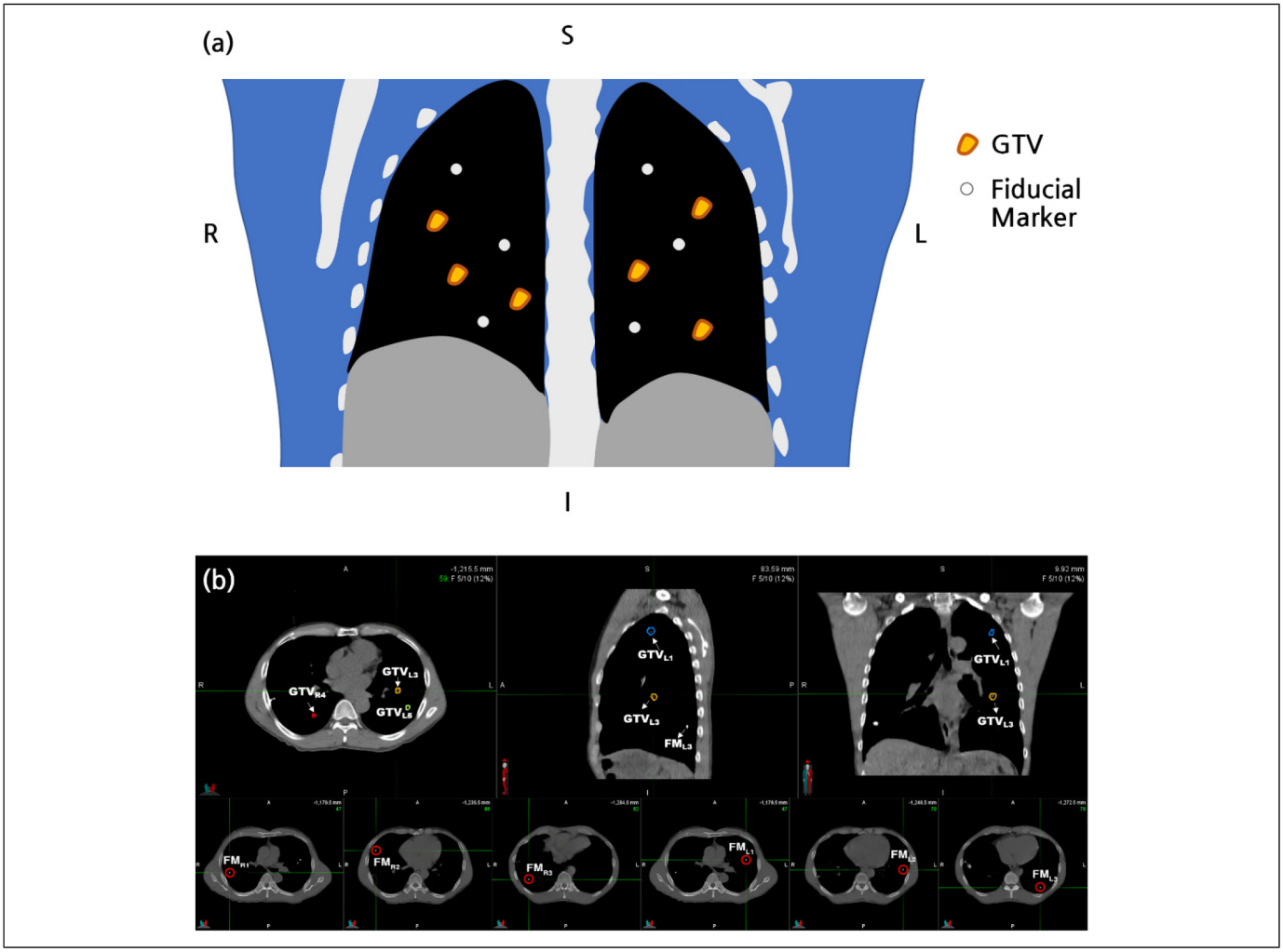

Figure 1. (a) Schematic and (b) patient CT images of perioperative fiducial implant for postoperative radiosurgery in the lung.

localization errors.[12–14] Therefore, to use the tumor tracking method with a limited number of FMs, uncertainties related to motion discrepancies between FMs and tumors should be quantified to be considered in the treatment planning.

In this field, a deformable image registration (DIR) algorithm is one of the feasible solutions for finding a correlation between the tumor positions and FMs in 4D CT images.[15–17] DIR algorithms have evolved over the last few decades and have been utilized to achieve specialized objectives, such as matching of images generated by homogeneous/heterogeneous modalities and dose accumulation, considering different motion/posture phases.[18,19] Moreover, DIR algorithms have been frequently utilized for the assessment of respiratory motion based on 4D CT images.[20–24] Several literature reports have also presented the accuracies of DIR algorithms in different cases, including the occurrence of high- and low-contrast regions[25–36] and multiorgan deformation.[37,38–40] Based on this information, various DIR algorithms have been implemented in commercial oncology software and treatment planning systems (eg, MIM [MIM Software Inc.] and RayStation [RaySearch Laboratories]) and are being used for practical purposes.[41]

Yeo et al[36] quantitatively investigated the accuracy of various DIR algorithms in terms of the displacement of FMs and tumors in the low-contrast regions of images. They also evaluated the deformation performance of DIR algorithms using a deformable phantom. Based on the literature,[36] the DIR methods have been already used clinically for lung cases. Unfortunately, these DIR algorithms were not quantitatively evaluated using the CT data of patients who received perioperative FM implant in the lungs to treat multiple lung metastases using postoperative radiosurgery.[11] Accordingly, evaluating the trajectory correlation between FMs and tumors in tumor-tracking radiation therapy is necessary using implanted FMs. Thus, in this study, we evaluated the tracking performance of 10 DIR algorithms for FMs and tumors using 4D CT images of 5 patients with multiple lung metastases.

Materials and Methods

Patients and 4D CT Images

This study was approved by the institutional review board of the Severance Hospital (4-2020-0311), and all methods were performed under relevant guidelines and regulations. The requirement for informed consent waived with the approval of the ethics committee given that patient anonymity was ensured.

The 4D CT images of 5 consecutive patients with intraoperative FM implant were retrospectively evaluated in this study. Patient characteristics are summarized in Table 1. The number of multiple metastatic tumor lesions (gross tumor volume) in the lungs varied among the patients (range: 1-10). Four to six FMs were implanted for each patient during the surgery performed prior to radiation therapy. A maximum of 3 FMs were implanted in each of the right and left lobes. In general, one FM was implanted into each of the upper, middle, and lower lobes of the lung. The number of implanted FMs was determined during surgery by the surgeon considering the number and location of the tumor and patient factors. Figure 1 shows a schematic illustration and representative CT image with 6 FMs.

Patients were set up in the head-first supine position and immobilized using a vacuum BodyFix® (BodyFix, Elekta AB) and Kneefix™ (CIVCO, Civco Medical Solutions). For respiratory motion control, all 4D CT simulations were scanned with free breathing and continuous positive airway pressure (C-PAP). The C-PAP levels were set to 10 to 15 cmH_2O depending on the breathing condition of the patient. Under the consideration of clinical practice, the pixel resolution of CT images was approximately 1.0×1.0 mm^2, and the slice thickness of each image was fixed at 3.0 mm. All 4D CT images were acquired with a 16-slice scanner (Aquilion LB, Canon Medical Systems) using a respiratory monitoring system (Anzai, Anzai Medical) and retrospectively sorted (reconstructed) into 10-phase bins within the respiratory cycle. Table 1 provides information regarding the number of FMs and the tumors (or gross tumor volumes [GTVs]).

Table 2. List of the Deformable Image Registration (DIR) Algorithms Investigated in This Study.

Index	DIR Algorithm
A	Original Horn and Schunck[45]
B	Combined Lucas Kanade and Horn and Schunck[46]
C	Inverse consistent Horn and Schunck[47]
D	Iterative optical flow method[43]
E	Fast demons[34]
F	Modified demons[48]
G	Original demons[44]
H	Original level set motion[49]
I	Affine approximation of level set motion[49]
J	Free-form deformation method[50]

Generation of the Ground-Truth From 4D CT

For the quantitative evaluation of the DIR algorithms, we compared the deformed position and its ground-truth position.[42] First, in this study, the end exhalation (T50) phase was set to the reference phase of 4D CT, and the ground-truth positions for tracking FMs and GTVs in 4D CT were generated from the reference phase to others (ie, T60, …, T0, …, T30, T40). Regarding the ground-truth, the trajectory of an FM was generated by following the position of the voxel that had the maximum Hounsfield unit (HU) value near the FM position of the previous phase, considering the smaller size of the FM as compared to the voxel resolution. A contour of GTVs was defined on each phase of the 4D CT by physicians based on their medical expertise, and subsequently, the trajectory of each GTV was estimated according to the center of mass of the tumor volumes (average volume of GTV <0.5 mL). The final contours used in the analysis were reviewed by the same experienced physician to avoid inter-physician bias. The uncertainty of the ground-truth position was within $1.00 \times 1.00 \times 3.00$ mm^3, which is as much as the voxel resolution used in this study.

Assessment of DIR Algorithms

This study aims to evaluate whether the previous phantom-based research could be applied to a real patient image in clinical practice. For this, a total of 10 DIR algorithms were investigated, selected by considering the results obtained by Yeo et al[36]: 4 optical flow algorithms,[43] 3 demon algorithms,[44] 2 level-set motion algorithms, and 1 free-form deformation algorithm. Based on the results reported in the literature,[36] an algorithm in which FMs would not be identifiable (ie, b-spline) and the worst demons algorithm producing significantly incorrect deformation results (ie, double force demons) were excluded in this study. Table 2 lists the DIR algorithms investigated in this study.

All DIR algorithms listed in Table 2 were implemented by the Deformable Image Registration and Adaptive Radiotherapy (DIRART) software.[51] Four multigrid stages were used ($n = 1$ to 4) with $10n$ iterations per pass to establish the optimum DIR performance.[36] The DIRART software has been widely used in research and clinical areas with respect to image registration study to this day.[36,52–54] The DIRs were calculated without any postprocessing methods, such as smoothing, and the results were extracted as an array type, including deformation vector fields (DVFs) generated by DIR for the calculation of voxel movements. For performing DIR, the reference phase (ie, T50) and other phases (T60, T70, …, T30, and T40) were selected as a moving image and fixed images, respectively. The entire field of view of the CT image was selected as a region of interest of DIR.

Each deformed position of the FMs and GTVs was collected by direction vectors extracted from the DVF corresponding to the index of the maximum HU value and the center of mass of the GTV in the reference phase, respectively. Subsequently, for the evaluation of the DIR performance, the results obtained by the 10 DIR algorithms were compared, in terms of the target registration error (TRE), with the ground-truth generated, as detailed in the section "Generation of the Ground-Truth From 4D CT".

Results

Assessment of the Deformed Images According to the DIR Algorithms

Figure 2 presents an example of deformed images according to each of the 10 DIR algorithms (top) and their difference maps compared with the original fixed image (bottom). Qualitatively, our results indicate that the images deformed

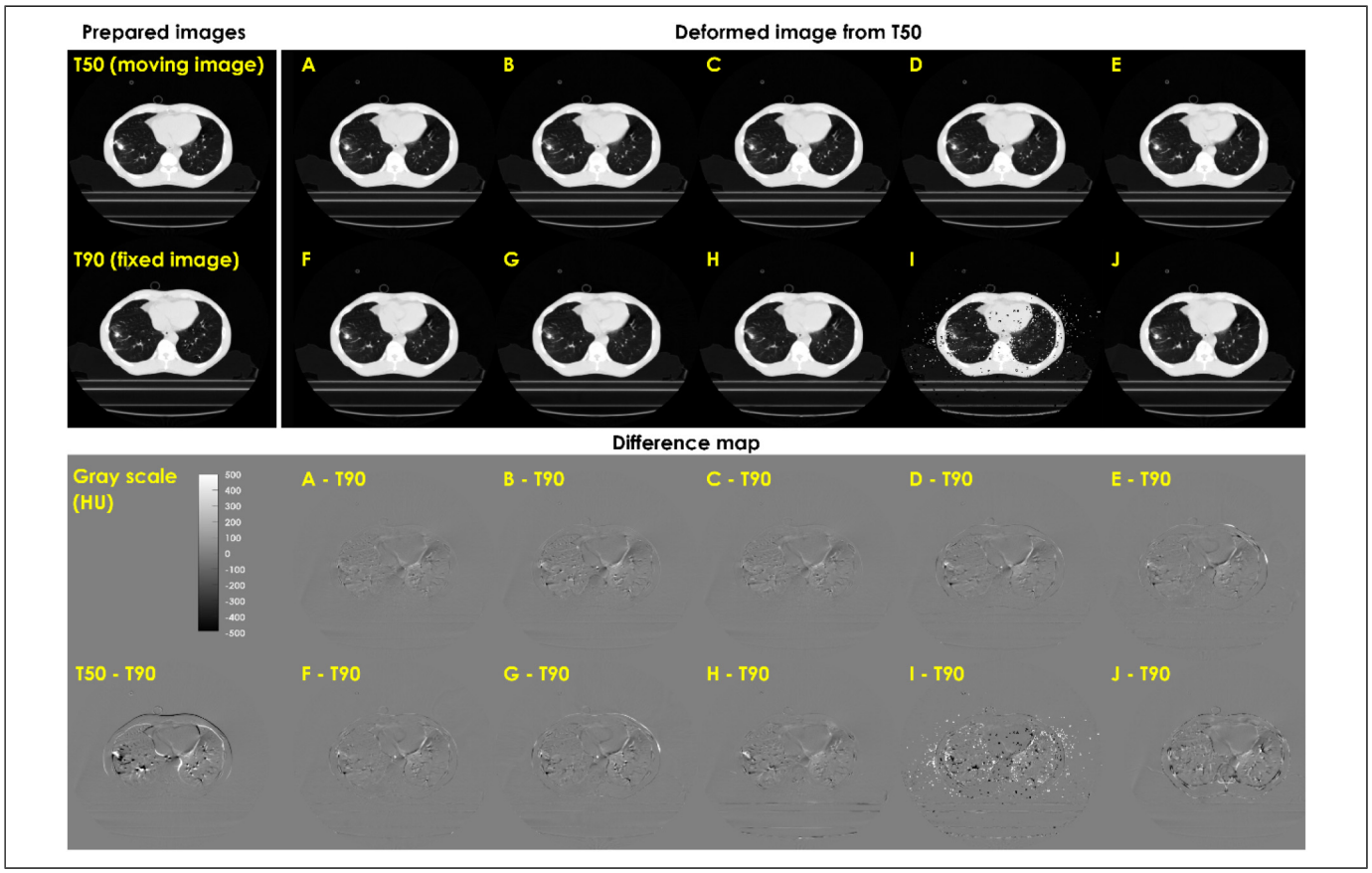

Figure 2. Example of deformed images according to 10 deformable image registration (DIR) algorithms (top) and their difference maps compared with the original fixed image (bottom). The DIR algorithms are listed in Table 2.

by optical flow algorithms (Algorithms A–D) and demons algorithms (Algorithms E–G) were reasonably well deformed. The images deformed by other algorithms were slightly (Algorithms H) or fairly (Algorithms I–J) different from the original fixed image (Figure 2).

Assessment of the Deformed Position for FMs

Figure 3 details the TREs of the X, Y, Z, and 3D displacements between the ground-truth and estimated positions obtained using the DIR algorithms for FM movements. In the figure, the optical flow methods (Algorithms A–D) delivered better tendency regardless of the position of FMs, and the mean and standard deviations of TREs were in the range of 1.82 ± 1.05 mm (best performance, Algorithm D) to 1.98 ± 1.17 mm (worst performance, Algorithm B). These errors were within the uncertainty of the ground-truth. With respect to the demons algorithms (Algorithms E–G), the TREs were slightly higher (2.23 ± 2.78 [Algorithm F] to 3.41 ± 4.42 mm [Algorithm G]) than those of the optical flow algorithms. In other DIR algorithms (Algorithms H–J), considerable differences were observed between the ground-truth and deformed positions, varying from 5.43 ± 7.82 mm (Algorithm I) to 7.11 ± 9.76 mm (Algorithm J).

Assessment of the Deformed Position for Tumors

Figure 4 presents the TREs of the X, Y, Z, and 3D displacements between the ground-truth and estimated positions obtained using the DIR algorithms for GTV movements. Figure 4 indicates the reasonable results obtained by the optical flow methods (Algorithms A–D). These results are comparable to the previous FM results, where the mean and standard deviations of TREs ranged from 1.29 ± 1.21 mm (best performance, Algorithm D) to 1.64 ± 1.22 mm (worst performance, Algorithm B). These deformation errors were within

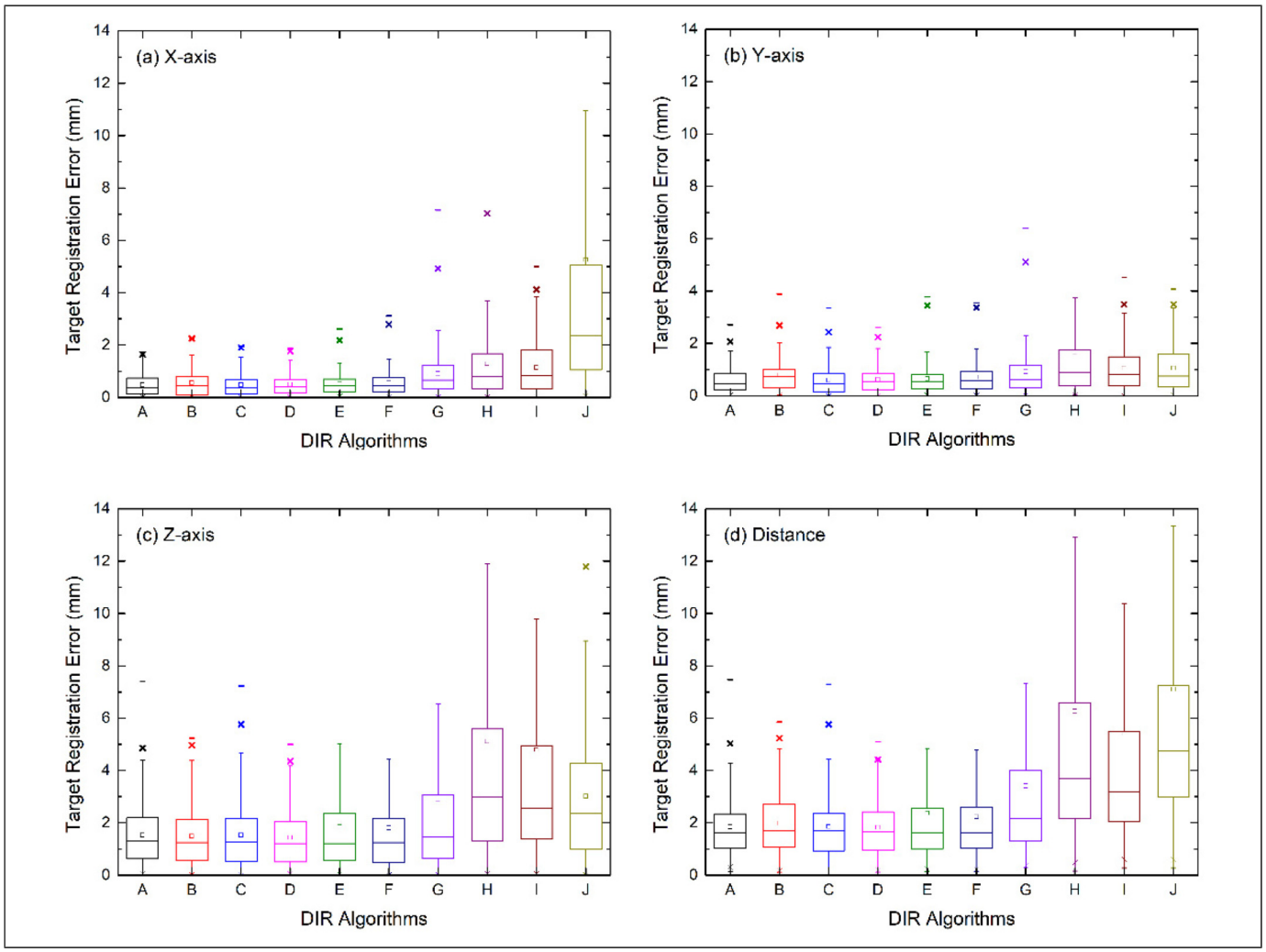

Figure 3. Comparison of the target registration errors (TREs) between the ground-truth and the DIR results for fiducial marker (FM) movements: (a) *X*-axis, (b) *Y*-axis, (c) *Z*-axis, and (d) distance in the 3D coordinate space. The DIR results were obtained from 9 images deformed from the reference phases (ie, T50) of 5 patients, and outliers over the 14 mm range were not visualized.

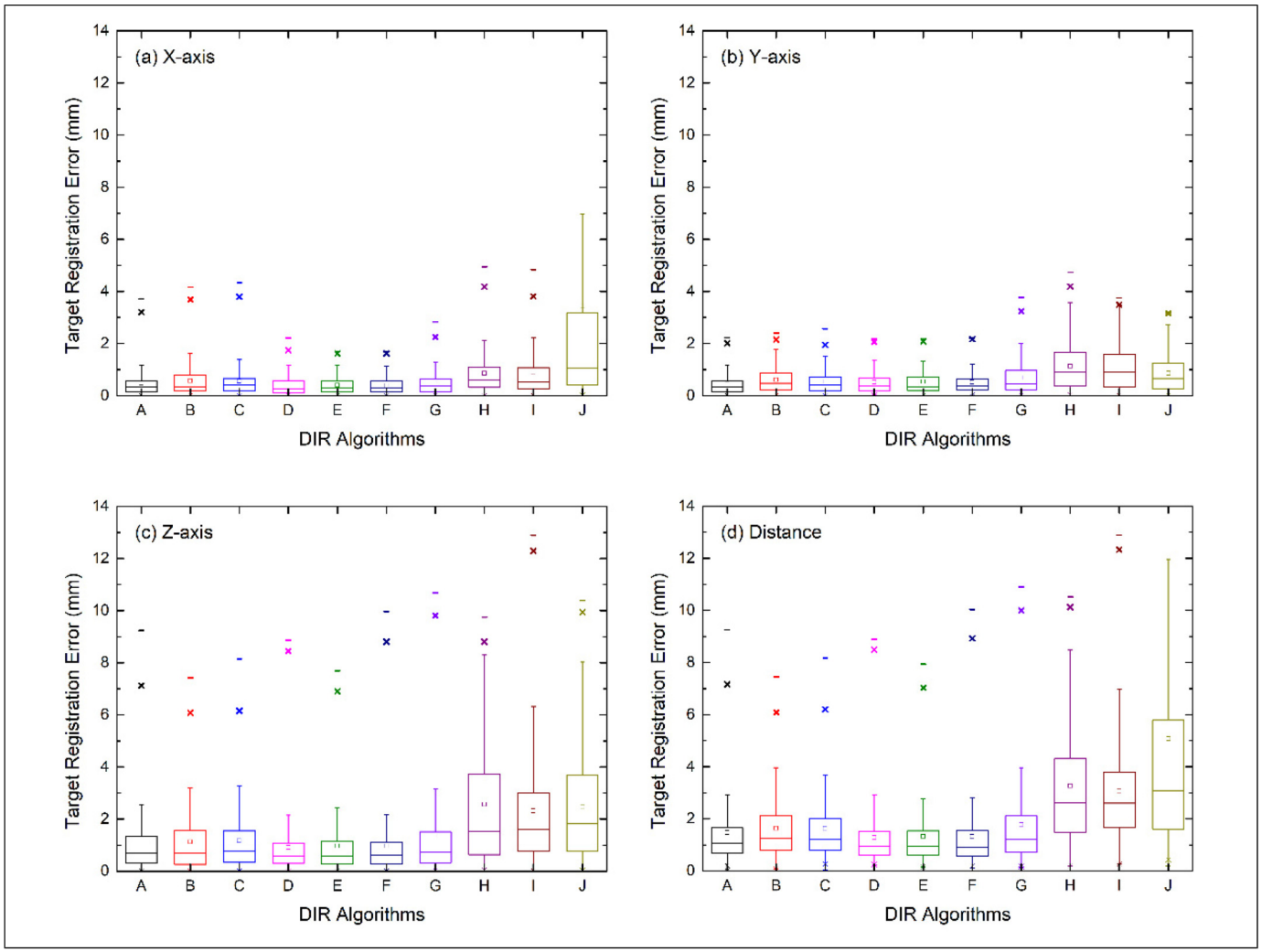

Figure 4. Comparison of the target registration errors (TREs) between the ground-truth and the DIR results for GTV movements: (a) *X*-axis, (b) *Y*-axis, (c) *Z*-axis, and (d) distance in the 3D coordinate space. The DIR results were obtained from 9 images deformed from the reference phases (ie, T50) of 5 patients, and outliers over the 14 mm range were not visualized.

the uncertainty of the ground-truth. With respect to the demons algorithms (Algorithms E–G), the TREs showed better tendency than before, ranging from 1.32 ± 1.22 mm (Algorithm E) to 1.78 ± 1.75 mm (Algorithm G)), which has a similar level of error to that in the case of the optical flow methods. In other cases (ie, Algorithms H–J), the TREs were slightly lower than those of the previous FM results but still higher than those of the optical flow and demons algorithms, varying from 3.07 ± 2.16 mm (Algorithm I) to 5.07 ± 9.33 mm (Algorithm J).

Discussion

The deformed images obtained by the 10 DIR algorithms exhibited the same trends in all patient images, and our results show that the deformed positions obtained using Algorithms A–F were well estimated within the uncertainty of the tested CT resolution. Here, Algorithm D showed the best performance. Our results were similar to those observed in a prior study on phantom images conducted by Yeo et al.[36] Nevertheless, a few outliers were detected in real patient cases.

With respect to the deformed position of FMs, in the 2 DIR algorithm groups, that is, optical flow and demons, the maximum TREs were observed owing to the large discrepancy between the HU values in fixed and moving images. Figure 5 presents an example of outlier results deformed by the original Horn and Schunck optical flow algorithm (Algorithm A). As illustrated in Figure 5a and b, the HU values of the FM included in the fixed image (ie, T30) were relatively lower than those of the moving image (ie, T50), and this HU discrepancy caused the DIR error. In this case, the voxels had to move somewhere, not the ground-truth position, and consequently, TREs would be higher than those in general situations. In Figure 5, the maximum TREs were 2.79 to 4.05 times higher than the mean TREs for all optical flow algorithms. Particularly, when outlier cases that had unclear FMs in 4D CT images were

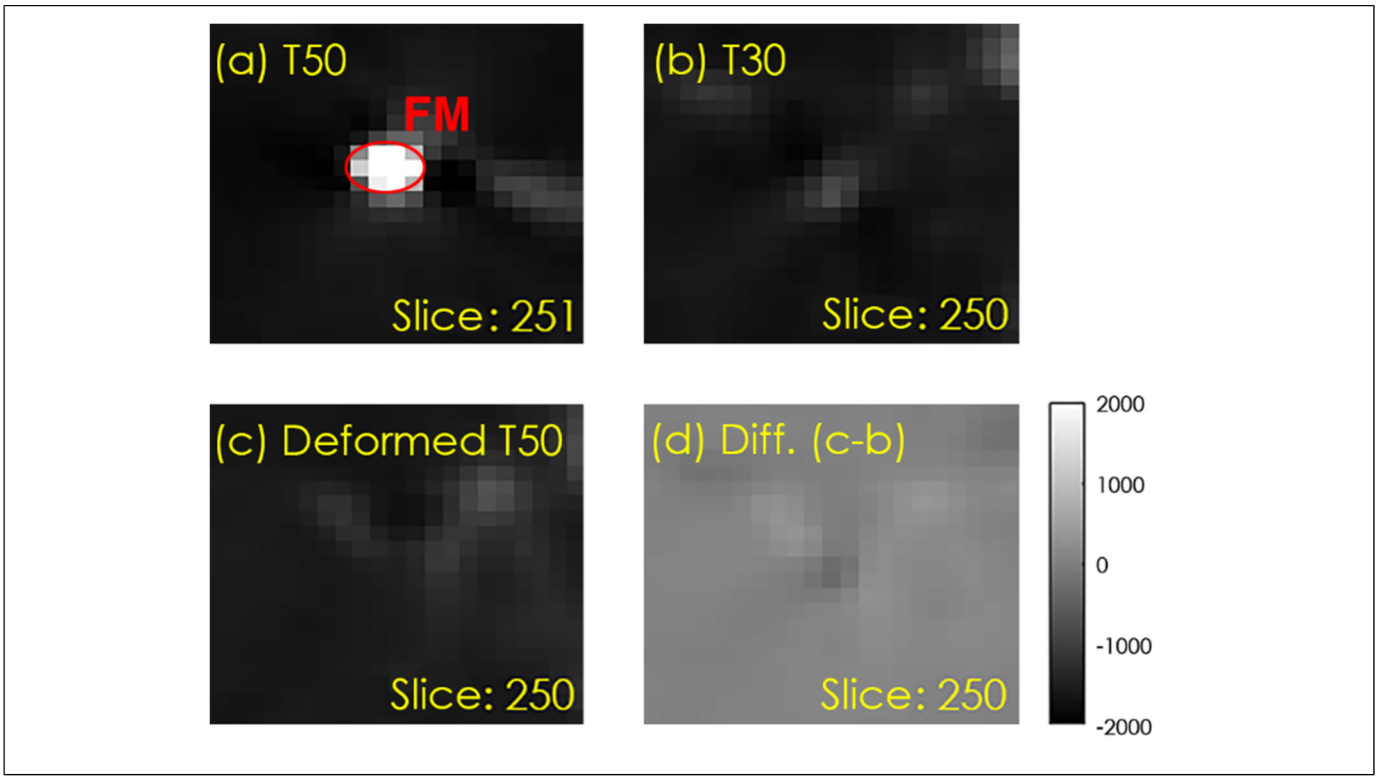

Figure 5. Sample outlier results deformed by the original Horn and Schunck optical flow method (Algorithm A). (a) T50, (b) T30, (c) deformed T50, and (d) the difference between (c) and (b). The red contour in (a) shows a fiducial marker (FM), but the FM is unclear in (b).

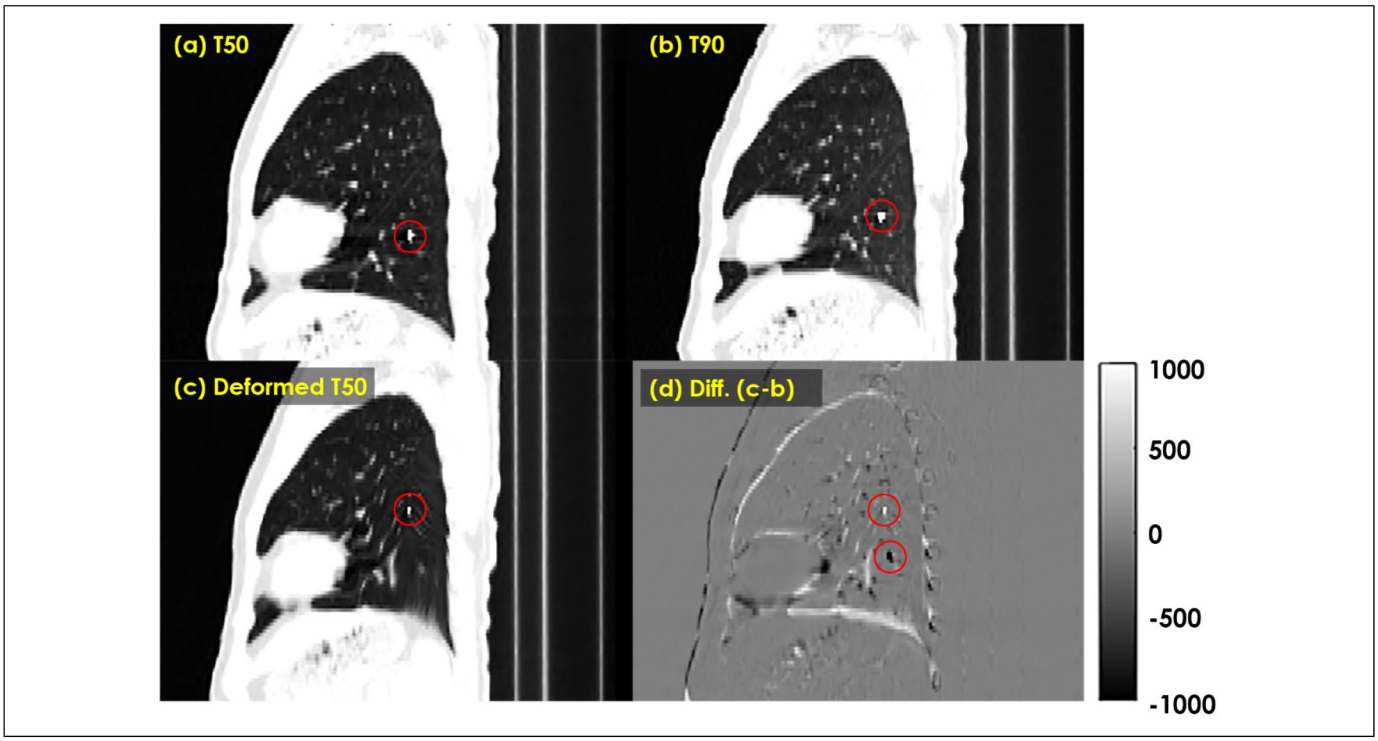

Figure 6. Sample outlier results deformed by the fast demons algorithm (Algorithm E). (a) T50, (b) T90, (c) deformed T50, and (d) the difference between (c) and (b). The red contours in (a)–(c) show the different positions of an identical fiducial marker (FM) inserted in the patient.

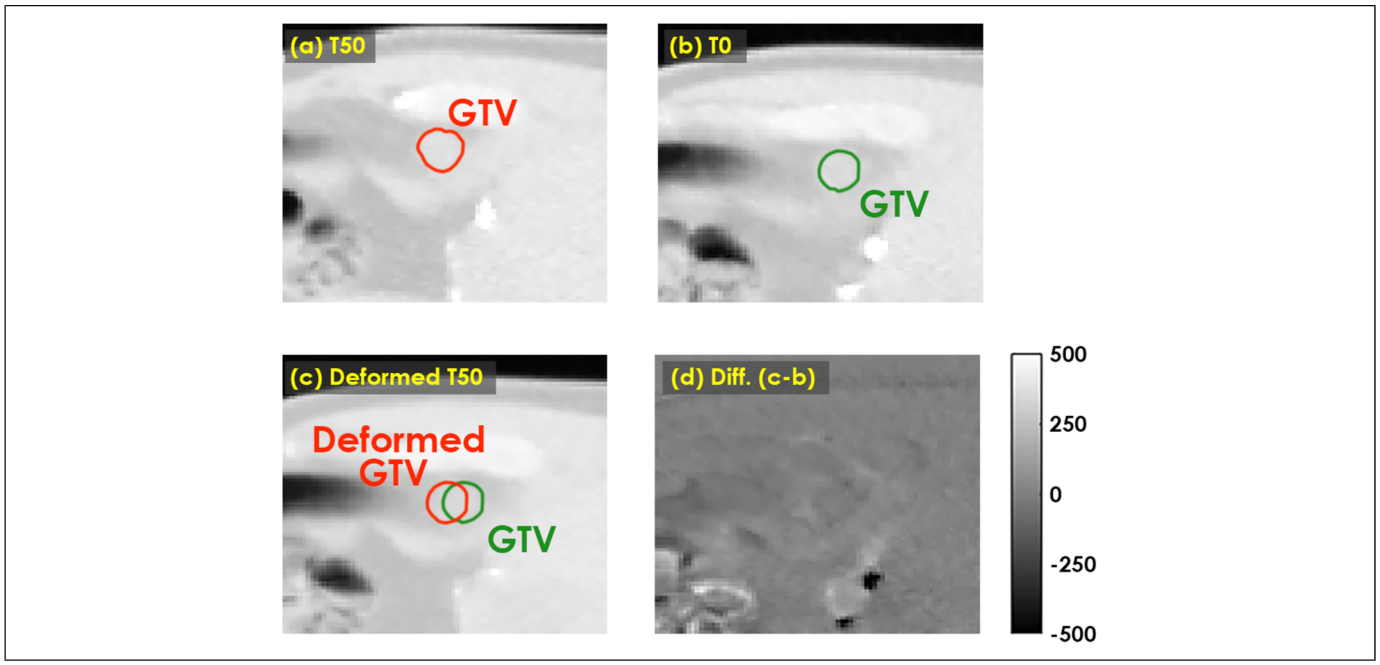

Figure 7. Sample case of DIR errors with similar Hounsfield unit (HU) values between the gross tumor volume (GTV) and nearby normal tissues. In this figure, slices of 4-dimensional computed tomography (4D CT) images for (a) T50 and (b) T0 show an indistinguishable GTV. Hence, DIR could not clearly define the GTV deformation in the (c) deformed T50; (d) shows the difference between (c) and (b) images. Contour lines in (a) and (b) represent the GTV region, and red and green lines in (c) represent the deformed GTV and GTV at T0, respectively.

excluded in these samples, the mean, standard deviation, and maximum TREs of the results deformed by the iterative optical flow method were extremely better than before, with values of 1.07, 0.60, and 2.92 mm, respectively. In the clinical approach, FMs may not appear (or appear faintly) in 4D CT images, depending on the status of the 4D CT machine and its configuration (eg, slice thickness and slice increment). This condition would be overcome using an interpolation method between 2 well-deformed results.

Figure 6 presents an example of another outlier result deformed by the fast demons (Algorithm E) algorithm. Even if FMs were well and clearly defined in moving (Figure 6a) and fixed (Figure 6b) images, under the demons algorithms, the deformation of the FM positions included in the deformed T50 (Figure 6c) was superior to that of the fixed image.

This trend in the deformation errors did not exhibit any significant difference, in comparison with the results obtained via DIR in phantoms reported by Yeo et al.[36] Hence, the limitations of the demons algorithms described in the literature apply not only to phantom images but also to patient CT images.

Considering the deformed positions for tumors, in the 2 DIR algorithm groups, that is, optical flow and demons, the maximum differences of the deformed positions for GTV tracking were approximately 4.55 to 7.55 times higher than the mean differences. Here, errors caused by the aforementioned difference in the HU values were also observed. As shown in Figure 7, when GTV was located at the diaphragm level, it was not clearly distinguished from adjacent normal tissues (ie, liver, stomach, bowel, and spleen), resulting in an error in GTV tracking. Consequently, even if the GTV position could be estimated by the DIR algorithms, the physician should carefully and manually check the position of the GTV in each phase.

The limitation of this study is that the DIR algorithms were evaluated only by using a limited number of patients' 4D CT images (ie, 5 4D-CT datasets). Nevertheless, the trend of the deformed results of more than 20 FMs and GTVs by the DIR algorithms was virtually similar to those of the previous phantom-based study.[36] Another limitation is that the DIR algorithm used in this study was not evaluated at different operational parameters. The parameters used in the detailed options of the DIR process were similar with those suggested by Yeo et al.[36] Hence, the limitations due to the parameters may be the same as those in the previous literature. Properly establishing the best parameters can improve the performance of the algorithm. Other parameters might have a possibility to bring better results than our results.

Conclusions

In this study, we quantitatively evaluated 10 common DIR algorithms in real 4D CT images of patients. The results for 2 categories, namely, FM and GTV, were compared with the ground-truth positions. Based on our results, the optical flow algorithms yielded reasonable results for FMs and GTVs, and the iterative optical flow algorithm yielded the best performance. The mean and standard deviations of TREs were 1.82 $\pm$ 1.05 mm for the FM position and 1.29 $\pm$ 1.21 mm for the GTV position. The estimations all the GTV positions had

some limitations. The demons algorithms exhibited large discrepancies between the deformed and fixed images with respect to FMs, and the other 2 algorithms (level-set motion and free-form deformation) had the worst results. Accordingly, we conclude that FM positions could be estimated using the best DIR algorithms, such as the iterative optical flow method, within the uncertainties of the CT resolution, with respect to the tumor position. However, the DIR algorithms could not be used to estimate several tumor positions tested in this study. Hence, deformed positions for a tumor might need to be manually checked by physicians. We expect that this limitation would be overcome in the near future with the use of advanced methods, such as AI-based techniques.

Acknowledgments

We thank the anonymous reviewers whose insightful comments and suggestions helped improve and clarify this manuscript.

Declaration of Conflicting Interests

The authors declared no potential conflicts of interest with respect to the research, authorship, and/or publication of this article.

Funding

The authors disclosed receipt of the following financial support for the research, authorship, and/or publication of this article: This work was supported by Radiation Technology R&D program through the National Research Foundation of Korea funded by the Ministry of Science and ICT (MSIT) (Project No.: NRF-2015M3A9E2067001, NRF-2020R1C1C1005713, NRF-2021R1I1A1A01057995), and supported by a faculty research grant of Yonsei University College of Medicine (6-2020-0154).

Ethics Statement

This study was approved by the institutional review board of the Severance Hospital (4-2020-0311), and all methods were performed under relevant guidelines and regulations. The requirement for informed consent waived with the approval of the ethics committee given that patient anonymity was ensured.

ORCID iD

Chae-Seon Hong https://orcid.org/0000-0001-9120-6132

References

1. Verellen D, Linthout N, van den Berge D, Bel A, Storme G. Initial experience with intensity-modulated conformal radiation therapy for treatment of the head and neck region. *Int J Radiat Oncol Biol Phys.* 1997;39(1):99-114. doi:10.1016/s0360-3016(97)00304-0
2. Verhey LJ. Comparison of three-dimensional conformal radiation therapy and intensity-modulated radiation therapy systems. *Semin Radiat Oncol*. 1999;9(1):78-98. doi:10.1016/s1053-4296(99)80056-3
3. Chao KS, Low DA, Perez CA, Purdy JA. Intensity-modulated radiation therapy in head and neck cancers: the Mallinckrodt experience. *Int J Cancer.* 2000;90(2):92-103. doi:10.1002/(sici)1097-0215(20000420)90:2<92::aid-ijc5>3.0.co;2-9
4. Intensity Modulated Radiation Therapy Collaborative Working G. Intensity-modulated radiotherapy: current status and issues of interest. *Int J Radiat Oncol Biol Phys*. 2001;51(4):880-914. doi:10.1016/s0360-3016(01)01749-7
5. Van Herk M, Remeijer P, Rasch C, Lebesque JV. The probability of correct target dosage: dose-population histograms for deriving treatment margins in radiotherapy. *Int J Radiat Oncol Biol Phys.* 2000;47(4):1121-1135. doi:10.1016/s0360-3016(00)00518-6
6. Keall PJ, Mageras GS, Balter JM, et al. The management of respiratory motion in radiation oncology report of AAPM Task Group 76. *Med Phys*. 2006;33(10):3874-3900. doi:10.1118/1.2349696
7. Rietzel E, Pan T, Chen GT. Four-dimensional computed tomography: image formation and clinical protocol. *Med Phys*. 2005;32-(4):874-889. doi:10.1118/1.1869852
8. Tang XL, Sharp GC, Jiang SB. Fluoroscopic tracking of multiple implanted fiducial markers using multiple object tracking. *Phys Med Biol.* 2007;52(14):4081-4098. doi:10.1088/0031-9155/52/14/005
9. Palma DA, Olson R, Harrow S, et al. Stereotactic ablative radiotherapy versus standard of care palliative treatment in patients with oligometastatic cancers (SABR-COMET): a randomised, phase 2, open-label trial. *Lancet.* 2019;393(10185):2051-2058. doi:10.1016/S0140-6736(18)32487-5
10. Pennathur A, Luketich JD, Heron DE, et al. Stereotactic radiosurgery for the treatment of stage I non-small cell lung cancer in high-risk patients. *J Thorac Cardiov Sur*. 2009;137(3):597-604. doi:10.1016/j.jtcvs.2008.06.046
11. Pop D, Venissac N, Bondiau PY, Mouroux J. Peroperative fiducial placement for postoperative stereotactic Cyberknife radiosurgery. *Interact Cardiovasc Thorac Surg*. 2010;10(6):1034-1036. doi:10.1510/icvts.2009.227348
12. Seppenwoolde Y, Shirato H, Kitamura K, et al. Precise and real-time measurement of 3D tumor motion in lung due to breathing and heartbeat, measured during radiotherapy. *Int J Radiat Oncol*. 2002;53(4):822-834. doi 10.1016/S0360-3016(02)02803-1
13. Seregni M, Pella A, Riboldi M, Orecchia R, Cerveri P, Baroni G. Real-time tumor tracking with an artificial neural networks-based method: a feasibility study. *Phys Med*. 2013;29(1):48-59. doi:10.1016/j.ejmp.2011.11.005
14. Takamiya M, Nakamura M, Akimoto M, et al. Multivariate analysis for the estimation of target localization errors in fiducial marker-based radiotherapy. *Med Phys*. 2016;43(4):1907. doi:10.1118/1.4944594
15. Lu WG, Olivera GH, Chen Q, Chen ML, Ruchala KJ. Automatic re-contouring in 4D radiotherapy. *Phys Med Biol.* 2006;51-(5):1077-1099. doi:10.1088/0031-9155/51/5/002
16. Von Siebenthal M, Szekely GA, Lomax AJ, Cattin PC. Systematic errors in respiratory gating due to intrafraction deformations of the liver. *Med Phys*. 2007;34(9):3620-3629. doi:10.1118/1.2767053
17. Samant SS, Xia J, Muyan-Ozcelik P, Owens JD. High performance computing for deformable image registration: towards a new paradigm in adaptive radiotherapy. *Med Phys*. 2008;35-(8):3546-3553. doi:10.1118/1.2948318

18. Heath E, Seco J. Dynamic beam delivery and 4D Monte Carlo. In: *Monte Carlo Tech Radiat Ther*. CRC Press; 2016:111–126.
19. Schnabel JA, Heinrich MP, Papiez BW, Brady SJM. Advances and challenges in deformable image registration: from image fusion to complex motion modelling. *Med Image Anal*. 2016;33(1):145-148. doi:10.1016/j.media.2016.06.031
20. Castillo E, Castillo R, Martinez J, Shenoy M, Guerrero T. Four-dimensional deformable image registration using trajectory modeling. *Phys Med Biol.* 2010;55(1):305-327. doi:10.1088/0031-9155/55/1/018
21. Han MC, Seo JM, Lee SH, et al. Continuously deforming 4D voxel phantom for realistic representation of respiratory motion in Monte Carlo dose calculation. *IEEE T Nucl Sci*. 2016;63-(6):2918-2924.
22. Han MC, Yeom YS, Kim CH, Kim S, Sohn JW. New approach based on tetraedral-mesh geometry for accurate 4D Monte Carlo patient-dose calculation. *Phys Med Biol.* 2015;60(4):1601-1612. doi:10.1088/0031-9155/60/4/1601
23. Serban M, Heath E, Stroian G, Collins DL, Seuntjens J. A deformable phantom for 4D radiotherapy verification: design and image registration evaluation. *Med Phys*. 2008;35(3):1094-1102. doi:10.1118/1.2836417
24. Yang DS, Lu W, Low DA, Deasy JO, Hope AJ, El Naqa I. 4D-CT Motion estimation using deformable image registration and 5D respiratory motion modeling. *Med Phys*. 2008;35(10):4577-4590. doi:10.1118/1.2977828
25. Castillo R, Castillo E, Guerra R, et al. A framework for evaluation of deformable image registration spatial accuracy using large landmark point sets. *Phys Med Biol.* 2009;54(7):1849-1870. doi:10.1088/0031-9155/54/7/001
26. Coselmon MM, Balter JM, McShan DL, Kessler ML. Mutual information based CT registration of the lung at exhale and inhale breathing states using thin-plate splines. *Med Phys*. 2004;31(11):2942-2948. doi:10.1118/1.1803671
27. Han SC, Lee SS, Kim MS, et al. Evaluation of Various deformable image registrations for point and volume variations. *J Korean Phys Soc*. 2015;67(1):218-223. doi:10.3938/jkps.67.218
28. Kadoya N, Fujita Y, Katsuta Y, et al. Evaluation of various deformable image registration algorithms for thoracic images. *J Radiat Res*. 2014;55(1):175-182. doi:10.1093/jrr/rrt093
29. Li X, Zhang YY, Shi YH, et al. Comprehensive evaluation of ten deformable image registration algorithms for contour propagation between CT and cone-beam CT images in adaptive head & neck radiotherapy. *Plos One*. 2017;12(4):1–17. doi:ARTN e017590610.1371/journal.pone.0175906
30. Lu WG, Olivera GH, Chen Q, et al. Deformable registration of the planning image (kVCT) and the daily images (MVCT) for adaptive radiation therapy. *Phys Med Biol*. 2006;51(17):4357-4374. doi:10.1088/0031-9155/51/17/015
31. Moriya S, Tachibana H, Kitamura N, Sawant A, Sato M. Dose warping performance in deformable image registration in lung. *Phys Medica*. 2017;37(1):16-23. doi:10.1016/j.ejmp.2017.03.016
32. Nobnop W, Chitapanarux I, Neamin H, Wanwilairat S, Lorvidhaya V, Sanghangthum T. Evaluation of deformable image registration (DIR) methods for dose accumulation in nasopharyngeal cancer patients during radiotherapy. *Radiol Oncol*. 2017;51(4):438-446.
33. Sarrut D, Baudier T, Ayadi M, Tanguy R, Rit S. Deformable image registration applied to lung SBRT: usefulness and limitations. *Phys Medica*. 2017;44(1):108-112. doi:10.1016/j.ejmp.2017.09.121
34. Wang H, Dong L, O'Daniel J, et al. Validation of an accelerated 'demons' algorithm for deformable image registration in radiation therapy. *Phys Med Biol*. 2005;50(12):2887-2905. doi:10.1088/0031-9155/50/12/011
35. Wu X, Fu D, de la Zerda A, et al. Patient alignment and target tracking in radiosurgery of soft-tissue tumors using combined fiducial and skeletal structures tracking techniques. In: Urschel HC, Kresl JJ, Luketich JD, Papiez L, Timmerman RD, Schulz RA, eds. *Treating Tumors That Move with Respiration*. Springer Berlin Heidelberg; 2007:31-36.
36. Yeo UJ, Supple JR, Taylor ML, Smith R, Kron T, Franich RD. Performance of 12 DIR algorithms in low-contrast regions for mass and density conserving deformation. *Med Phys*. 2013;40(10):1–12. doi:10.1118/1.4819945
37. Schnabel JA, Tanner C, Castellano-Smith AD, et al. Validation of nonrigid image registration using finite-element methods: application to breast MR images. *IEEE T Med Imaging*. 2003;22(2):238-247. doi:10.1109/Tmi.2002.808367
38. Zhong HL, Kim J, Chetty IJ. Analysis of deformable image registration accuracy using computational modeling. *Med Phys*. 2010;37(3):970-979. doi:10.1118/1.3302141
39. Zhong HL, Kim J, Li HS, Nurushev T, Movsas B, Chetty IJ. A finite element method to correct deformable image registration errors in low-contrast regions. *Phys Med Biol.* 2012;57-(11):3499-3515. doi:10.1088/0031-9155/57/11/3499
40. Zhong HL, Peters T, Siebers JV. FEM-based evaluation of deformable image registration for radiation therapy. *Phys Med Biol.* 2007;52(16):4721-4738. doi:10.1088/0031-9155/52/16/001
41. Motegi K, Tachibana H, Motegi A, Hotta K, Baba H, Akimoto T. Usefulness of hybrid deformable image registration algorithms in prostate radiation therapy. *J Appl Clin Med Phys*. 2019;20(1):229-236. doi:10.1002/acm2.12515
42. Liu F, Hu Y, Zhang Q, Kincaid R, Goodman KA, Mageras GS. Evaluation of deformable image registration and a motion model in CT images with limited features. *Phys Med Biol*. 2012;57-(9):2539-2554. doi:10.1088/0031-9155/57/9/2539
43. Barron JL, Fleet DJ, Beauchemin SS. Performance of optical-flow techniques. *Int J Comput Vision*. 1994;12(1):43-77.
44. Thirion JP. Image matching as a diffusion process: an analogy with Maxwell's demons. *Med Image Anal*. 1998;2(3):243-260. doi: https://doi.org/10.1016/S1361-8415(98)80022-4
45. Horn BKP, Schunck BG. Determining optical-flow. *Artif Intell*. 1981;17(1-3):185-203.
46. Bruhn A, Weickert J, Schnorr C. Lucas/Kanade meets Horn/Schunck: combining local and global optic flow methods. *Int J Comput Vision*. 2005;61(3):211-231.
47. Yang D, Li H, Low DA, Deasy JO, El Naqa I. A fast inverse consistent deformable image registration method based on symmetric optical flow computation. *Phys Med Biol*. 2008;53(21):6143-6165.

48. Yeo BT, Sabuncu MR, Vercauteren T, Ayache N, Fischl B, Golland P. Spherical demons: fast diffeomorphic landmark-free surface registration. *IEEE Trans Med Imaging*. 2010;29(3):650-668. doi:10.1109/TMI.2009.2030797
49. Varadhan R, Karangelis G, Krishnan K, Hui S. A framework for deformable image registration validation in radiotherapy clinical applications. *J Appl Clin Med Phys*. 2013;14(1):192-213. doi: DOI 10.1120/jacmp.v14i1.4066
50. Lu WG, Chen ML, Olivera GH, Ruchala KJ, Mackie TR. Fast free-form deformable registration via calculus of variations. *Phys Med Biol.* 2004;49(14):3067-3087. doi:10.1088/0031-9155/49/14/003
51. Yang D, Brame S, El Naqa I, et al. Technical note: DIRART--A software suite for deformable image registration and adaptive radiotherapy research. *Med Phys*. 2011;38(1):67-77. doi:10.1118/1.3521468
52. Nobnop W, Chitapanarux I, Wanwilairat S, Tharavichitkul E, Lorvidhaya V, Sripan P. Effect of deformation methods on the accuracy of deformable image registration from kilovoltage CT to tomotherapy megavoltage CT. *Technol Cancer Res Treat*. 2019;18(1):1–9. doi:10.1177/1533033818821186
53. Novak V, Ptacek J, Fiala P, Vlachova Z, Jaskova P. Development and performance assessment of an advanced Lucas-Kanade algorithm for dose mapping of cervical cancer external radiotherapy and brachytherapy plans. *J Appl Clin Med Phys*. 2021;22(5):69-78. doi:10.1002/acm2.13249
54. Shin DS, Kang SH, Kim KH, et al. Development of a deformable lung phantom with 3D-printed flexible airways. *Med Phys*. 2020;47(3):898-908. doi:10.1002/mp.13982